

## Article

# Synergistic Effect of *Benincasa hispida* Peel Extract and KI on the Corrosion Inhibition of Mild Steel in HCl

Qihui Wang <sup>1,\*</sup> , Chongkang Zhao <sup>1</sup>, Qi Zhang <sup>1</sup>, Xing Zhou <sup>1</sup>, Zhitao Yan <sup>1</sup>, Yi Sun <sup>1</sup> , Da Sun <sup>2,\*</sup>  and Xueming Li <sup>3</sup>

<sup>1</sup> School of Civil Engineering and Architecture, Chongqing University of Science and Technology, Chongqing 401331, China; 2021206071@cqust.edu.cn (C.Z.); 2021206083@cqust.edu.cn (Q.Z.); yzt@cqust.edu.cn (Z.Y.); sunyi@cqust.edu.cn (Y.S.)

<sup>2</sup> Institute of Life Science & Biomedical Collaborative Innovation Center of Zhejiang Province, Zhejiang Provincial Key Laboratory for Water Environment and Marine Biological Resources Protection, National & Local Joint Engineering Research, Center for Ecological Treatment Technology of Urban Water Pollution, Wenzhou University, Wenzhou 325035, China

<sup>3</sup> School of Chemistry and Chemical Engineering, Chongqing University, Chongqing 400044, China; xuemingli@cqu.edu.cn

\* Correspondence: qihuiwang@cqust.edu.cn (Q.W.); sunday@wzu.edu.cn (D.S.); Tel.: +86-157-2325-0306 (Q.W.); +86-173-6586-6501 (D.S.)

**Abstract:** This study employed *Benincasa hispida* peel as a raw material for the preparation of *Benincasa hispida* peel extract (BHPE) via hot water extraction and freeze-drying processes. The synergistic effect of BHPE and KI on the corrosion inhibition of mild steel in 1 M HCl was investigated. The compositional analysis shows that BHPE consists mainly of a mixture of sugars, characterized by a high density of hydroxyl groups and unsaturated functional groups, characteristic of highly effective corrosion inhibitors. Electrochemical experiments and surface analysis show that the composite of BHPE and KI can effectively provide protection to mild steel. Moreover, the synergistic coefficient of BHPE and KI under various concentration conditions was greater than 1, and the highest corrosion inhibition efficiency was 94.4%. In addition, the corrosion inhibition mechanism of BHPE was thoroughly investigated using quantum chemistry (QC) and molecular dynamics simulation (MDS).

**Keywords:** corrosion inhibition; synergism; agricultural crops; mild steel



**Citation:** Wang, Q.; Zhao, C.; Zhang, Q.; Zhou, X.; Yan, Z.; Sun, Y.; Sun, D.; Li, X. Synergistic Effect of *Benincasa hispida* Peel Extract and KI on the Corrosion Inhibition of Mild Steel in HCl. *Sustainability* **2023**, *15*, 11370. <https://doi.org/10.3390/su151411370>

Academic Editor: Saviour A. Umoren

Received: 25 June 2023  
Revised: 15 July 2023  
Accepted: 20 July 2023  
Published: 21 July 2023



**Copyright:** © 2023 by the authors. Licensee MDPI, Basel, Switzerland. This article is an open access article distributed under the terms and conditions of the Creative Commons Attribution (CC BY) license (<https://creativecommons.org/licenses/by/4.0/>).

## 1. Introduction

Mild steel is widely utilized as an engineering material in various fields, including bridge construction, oil and gas exploration, and mechanical manufacturing, owing to its exceptional solderability and plasticity [1–5]. Despite these benefits, steel possesses highly reactive chemical properties, leading to potential rusting during production, processing, and usage, which can impact both its practical longevity and visual appearance [6–8]. Consequently, preventive measures must be implemented to mitigate rusting [9]. Acidic solutions are frequently used to eliminate impurities, such as oxide scale, rust, and welding slag from the steel surface, resulting in a clean, smooth base suitable for further processing and application [10–13]. However, the use of acid solutions can also harm the steel matrix, necessitating the use of corrosion inhibitors for effective functioning [14]. In recent times, plant extracts have gained attention as environmentally friendly and cost-effective corrosion inhibitors due to the numerous compounds present in them, such as alkaloids, amino acids, organic acids, monosaccharides, polysaccharides, and proteins, containing a significant amount of hydroxyl and unsaturated functional groups, which could inhibit metal corrosion [15–20]. However, the corrosion inhibition efficiency of a single plant extract may not be optimal, and combining it with other substances could increase its effectiveness [21–24].

The synergistic effect is characterized by the enhanced activity that occurs when two or more chemical substances interact, compared to their individual effects [25–27]. Halide ions ( $\text{Cl}^-$ ,  $\text{Br}^-$ ,  $\text{I}^-$ ) can act as bridges between the inhibitor molecules and the metal surface due to their high electronegativity, which makes it easier for the inhibitor molecules to adsorb on the metal surface [28,29]. Khadiri et al. [21] discovered that the combination of *Punica granatum* extract and KI significantly increased the corrosion inhibition of S355 steel in 1 M HCl solution. The study showed that the corrosion inhibition efficiency was maintained at 83% at 323 K. This was achieved through the enhancement of the interaction force between *Punica granatum* extract and the steel surface by KI. Similarly, Tang et al. [30] investigated the synergistic corrosion inhibition effect of *Mikania micrantha* extract and KI in 0.5 M  $\text{H}_2\text{SO}_4$  solution, and their study results showed that the synergistic coefficient (S) was greater than 1, with the inhibition efficacy maintained above 90% in the temperature range of 293 K to 323 K. Thomas et al. [23] also extracted corrosion inhibitors from *Garcinia indica* fruit rind using the reflux method and conducted a study on their synergistic corrosion inhibition mechanism with KI on mild steel in 1 M HCl. The research showed that the mixture of *Garcinia indica* fruit rind extract and KI was an efficient corrosion inhibitor, with  $\text{I}^-$  acting as a bridge between the inhibitor and the metal. However, the complex composition of plant extracts makes it challenging to explore their synergistic mechanism with KI and limits their use as corrosion inhibitors. Therefore, more research is necessary to comprehend the synergistic mechanism between plant extract corrosion inhibitors and KI.

*Benincasa hispida*, a commonly grown vegetable in Asian countries, including China, Japan, and India, is highly favored because of its low-calorie content, high fiber, and rich vitamin and mineral content [31,32]. Additionally, the vegetable plays a crucial role as a raw material in the food industry, owing to its many benefits, including low growing cost, high yield, and storage resistance [33]. Several products, such as beverages and jams, are made from it [34]. However, a large amount of *Benincasa hispida* rind waste is generated during food processing, which if recycled can provide environmental and economic advantages. At present, there is no report on the application of winter melon peel extract (BHPE) as a corrosion inhibitor. Therefore, it is of great theoretical and practical significance to understand the chemical composition of winter melon peel and investigate the corrosion inhibition mechanism of BHPE.

This study investigates the synergistic effect of BHPE and KI on mild steel corrosion inhibition in 1 M HCl. Initially, the main composition and functional groups of BHPE were determined using HPLC and FTIR. Then, the corrosion inhibition of mild steel was evaluated using electrochemical methods for BHPE, KI and BHP+KI combination. Additionally, scanning electron microscopy (SEM) and energy dispersive X-ray (EDX) were utilized to gather surface morphology and composition data. Finally, QC and MDS were conducted to explore the corrosion inhibition mechanism of BHPE. The experimental and theoretical data support that the combination of BHPE and KI has good corrosion inhibition performance, which provides new ideas for the research and utilization of plant corrosion inhibitors.

## 2. Materials and Methods

### 2.1. Material Preparation

The metals utilized in the experimentation comprise mild steel with a chemical composition of 1.8% C, 0.19% Si, 1.29% Mn, 0.014% P, 0.003% S, and 98.323% Fe. The KI reagent was purchased from Tianjin Zhiyuan Chemical Reagent Co. The *Benincasa hispida* utilized in the study was obtained from a local market, and the fruit skin was collected using a small knife. The working electrodes were sanded with SiC sandpaper of various grit sizes, including 800#, 1500#, 3000#, and 7000#. Ultrapure water was used to prepare 1 M HCl. All reagents used in the experiments were analytically pure.

## 2.2. Preparation and Characterization of BHPE

The collected *Benincasa hispida* peels were cleansed three times with ultrapure water and then dried in an oven at 70 °C for 24 h. Afterwards, the peel was added to 800 mL of distilled water and boiled for 4 h. The resulting solution was filtered and the volume was reduced to 40 mL. The solution was then dried in a lyophilizer at −60 °C for 72 h to obtain a brown BHPE powder.

In the present investigation, we utilized a Shimadzu LC-20AD high-performance liquid chromatograph (HPLC) to determine the monosaccharide content in the BHPE samples. The chromatographic column used in this process was composed of C 18 (4.6 × 200 mm, 5 μm) and was controlled at a temperature of 313 K. The mobile phase was prepared by mixing 0.05 M of potassium dihydrogen phosphate solution and acetonitrile in an 83:17 ratio, and the flow rate was set at 1.0 mL/min. The injection volume was 10 μL, and the detection wavelength was set to 250 nm. Moreover, the BHPE functional groups were characterized using Fourier transform infrared spectroscopy (FTIR) (Nicorette & Co. iS50, Wisconsin, USA), with the FTIR measurements taken in the range of 400–4000 cm<sup>−1</sup>.

## 2.3. Electrochemical Testing

All electrochemical experiments in this study were performed at the CHI 660 electrochemical workstation. The working electrode was mild steel encapsulated by epoxy resin to expose an exposed area of 1.0 cm<sup>2</sup>. The reference electrode was Ag/AgCl and the counter electrode was a Pt sheet.

The open circuit potential test time was 1200 s. The frequency range for the electrochemical impedance spectroscopy (EIS) test was limited to 100 kHz to 10 mHz, with a perturbation potential of ±10 mV. ZSimDemo software (version 3.30, AMETEK, Berwyn, PA, USA) was used to analyze the EIS data. The polarization curve test utilized a scan rate of 1 mV/s and a scan range of ±250 mV relative to the open circuit potential. All electrochemical tests were performed at 298 K.

## 2.4. Surface Analysis

The size of the mild steel sample for surface analysis was 0.5 cm × 0.5 cm × 0.5 cm. Immersed for 2 h in a 1 M HCl solution without or with a corrosion inhibitor. The specimens were soaked in ultrapure water and anhydrous ethanol, dried with cold air, and analyzed for surface morphology and EDX using a Quattro S scanning electron microscope from Thermo Fisher Scientific Inc (Waltham, MA, USA).

## 2.5. Theoretical Calculations

### 2.5.1. Quantum Chemical Computing (QC)

Density Flooding Theory (DFT) is a crucial theory utilized in predicting the reactivity and stability of compounds [35,36]. Using the B3LYP method in DFT, we optimized the geometric structures of the studied corrosion inhibitor molecules at the 6–311++ G (d, p) basis group level. Gaussian 09 W software calculated both the highest occupied and lowest unoccupied orbitals for the optimized corrosion inhibitor molecules.

### 2.5.2. Molecular Dynamics Simulation (MDS)

The effectiveness of the corrosion inhibitors was examined using MDS with the Force module of the Material Studio 2018 software [37]. The most representative adsorption surface, Fe (110), was chosen. The study included six 3D Fe models, each with dimensions of 6 × 6 × 6, 300 water molecules, and one molecule of the corrosion inhibitor. The COMPASS force field was used for the MDS, which employed a typical NVT ensemble with a time step of 1.0 fs and a total simulation time of 1000 ps. All the metal atoms were fixed during the calculations to ensure free interaction between the corrosion inhibitor molecule and the metal surface.

### 3. Results

#### 3.1. Characterization of Extract Composition

##### 3.1.1. FTIR Analysis

The corrosion inhibition potential of plant extracts is closely linked to the adsorption ability of their functional groups onto metal surfaces [38]. Organic compounds with heteroatoms, aromatic rings, and conjugated groups exhibit a greater likelihood of adsorption on metal surfaces, thereby playing a protective role against the corrosion of metals [39]. Thus, an FTIR analysis of BHPE was conducted to explore its functional group information. The FTIR spectrum is depicted in Figure 1. The peak at  $3420\text{ cm}^{-1}$  is ascribed to the stretching vibration of O–H or N–H of the intermolecular hydrogen bond; the peak at  $3157\text{ cm}^{-1}$  signifies the presence of unsaturated C–H bonding bonds [40]. The peaks at  $1624\text{ cm}^{-1}$  and  $1400\text{ cm}^{-1}$  correspond to the stretching vibrations of C=O and N–H, while the absorption band at  $1047\text{ cm}^{-1}$  represents the stretching vibrations of C–N bonds [41]. Finally, the peaks at  $824\text{ cm}^{-1}$  and  $531\text{ cm}^{-1}$  indicate the bending vibration of the N–H bond [42]. Therefore, these characteristic peaks establish the specific functional groups present in BHPE that demonstrate potential corrosion inhibition properties.

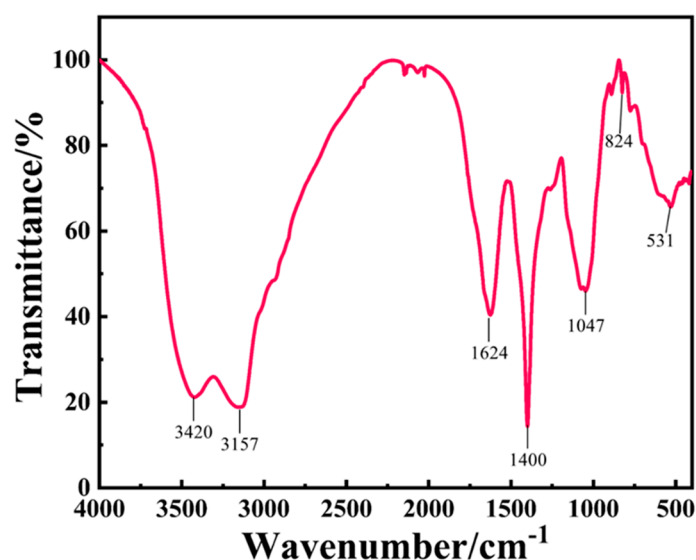


Figure 1. FTIR spectrum of BHPE.

##### 3.1.2. HPLC Analysis

To explicate the basic components of BHPE for theoretical calculations, we conducted HPLC analysis of the BHPE. Specifically, the HPLC spectra of BHPE are presented in Figure 2, while Table 1 contains information on the specific composition and content of BHPE. Figure 2 clearly shows that BHPE consists of 10 different monosaccharides, with the majority comprising D–Galactose and D (+)–Glucose, which account for 10.82% and 5.31%, respectively. Since glycan contains polar hydroxyl groups in their structure, they demonstrate enhanced affinity for metal surfaces, and enable the formation of adsorption films for corrosion inhibition purposes. Therefore, the potential corrosion inhibition properties of BHPE were reconfirmed by the HPLC results.

Table 1. Composition and content of BHPE.

Ingredient Name	Acronyms	Molecular Formula	CAS No.	Reserved Time (min)	Concent (%)
D–Mannose	DM	$C_6H_{12}O_6$	3458–28–4	14.18	0.83
D–Ribose	DR	$C_5H_{10}O_5$	50–69–1	18.59	0.26
L–Rhamnose	LP	$C_6H_{12}O_5$	3615–41–6	19.20	0.42

Table 1. Cont.

Ingredient Name	Acronyms	Molecular Formula	CAS No.	Reserved Time (min)	Concent (%)
D-Glucuronic acid	DGA	C <sub>6</sub> H <sub>10</sub> O <sub>7</sub>	6556-12-3	23.32	0.24
Trigalacturonic acid	TA	C <sub>18</sub> H <sub>26</sub> O <sub>19</sub>	6037-45-2	26.63	0.96
D (+)-Glucose	DG	C <sub>6</sub> H <sub>12</sub> O <sub>6</sub>	50-99-7	30.52	5.31
D-Galactose	DGT	C <sub>6</sub> H <sub>12</sub> O <sub>6</sub>	59-23-4	34.94	10.82
DL-Xylose	DLX	C <sub>5</sub> H <sub>10</sub> O <sub>5</sub>	25990-60-7	36.72	0.32
L-(+)-Ribose	LR	C <sub>5</sub> H <sub>10</sub> O <sub>5</sub>	147-81-9	38.15	0.66
D-(+)-Fucose	DF	C <sub>6</sub> H <sub>12</sub> O <sub>5</sub>	3615-37-0	43.65	0.15

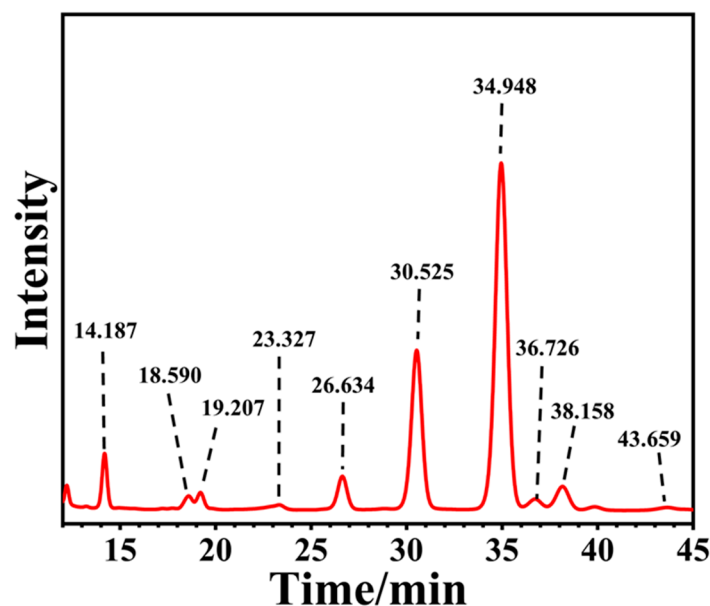


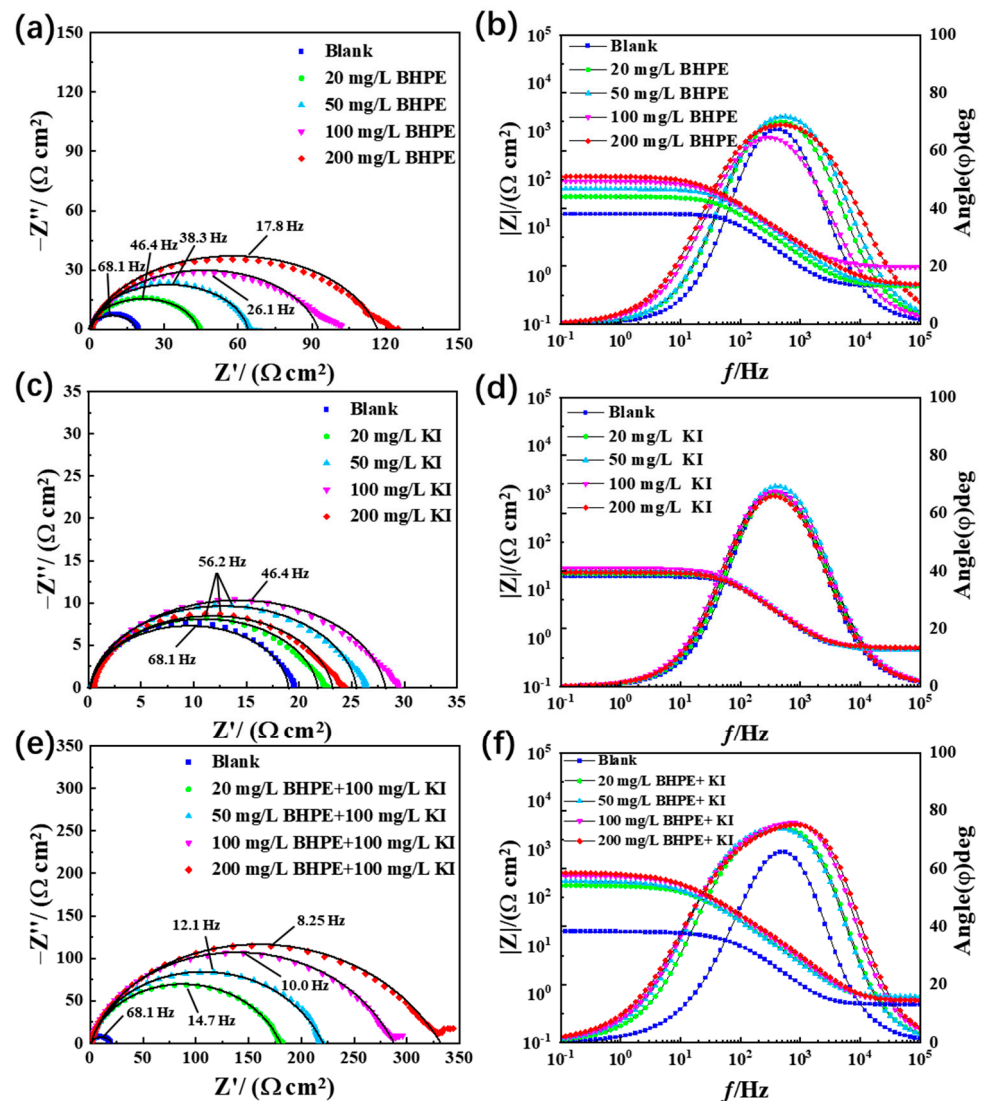
Figure 2. HPLC spectrum of BHPE.

### 3.2. Electrochemical Analysis

#### 3.2.1. EIS Analysis

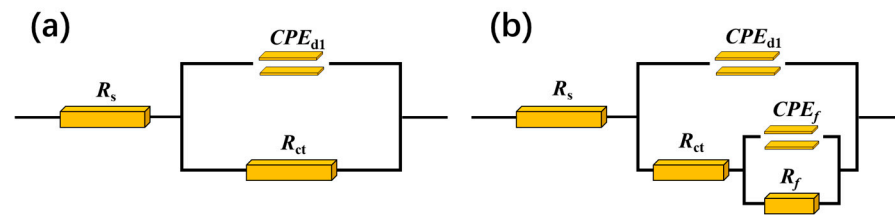
EIS tests were conducted to investigate the electrochemical mechanism of mild steel corrosion in 1 M HCl solution and evaluate the protective effect of BHPE and KI on mild steel. Figure 3 illustrates the Nyquist and Bode plots for the different corrosive solutions. The Nyquist plots depicted in Figure 3a,c,e show incomplete, flattened semicircles within the tested range that may have resulted from the non-uniformity of the electrode surface, commonly referred to as the “dispersion effect” [43]. The addition of various corrosion inhibitors did not alter the shape of the Nyquist plot, indicating that the charge transfer process is a significant contributor to controlling mild steel corrosion in HCl.

Figure 3a indicates that the radius of the capacitance arc gradually increases with the increase in BHPE concentration. This suggests that BHPE hinders the charge transfer process on the mild steel surface, thus slowing down the corrosion. Figure 3b shows a slight increase in the capacitance arc radius with the addition of KI, but it reaches a maximum at a concentration of 100 mg/L, suggesting that KI alone is not very effective in inhibiting corrosion. Therefore, 100 mg/L of KI was combined with different BHPE concentrations to study their corrosion inhibition effect. Figure 3c shows that the addition of I<sup>-</sup> doubles the radius of the capacitive arc at each BHPE concentration. This suggests that I<sup>-</sup> can significantly enhance the corrosion inhibition performance of BHPE.



**Figure 3.** Nyquist and Bode plots for mild steel in 1 M HCl without and with different corrosion inhibitors: (a,b) BHPE, (c,d) KI, (e,f) BHPE + 100 mg/L KI.

Figure 3b,d depict the Bode plots obtained from separate additions of BHPE and KI, respectively. The plots exhibit that the absolute impedance modulus in the low-frequency region and the maximum phase angle in the high-frequency region increase to some extent after the addition of BHPE. In contrast, KI only marginally increases these values after its addition. This observation suggests that BHPE and KI provide correlative inhibition against mild steel corrosion, with BHPE exhibiting higher inhibition performance compared to KI. Figure 3f demonstrates that the absolute impedance modulus increases remarkably when BHPE and KI are added together to the corrosive solution. This outcome substantiates that mild steel exhibits superior protection when BHPE–KI complex is added to the HCl solution. Notably, the simultaneous introduction of BHPE and KI alters the phase angle frequency relationship curve from a narrow peak to a broad peak, corresponding to a modification in the electrode reaction process from one time constant to two time constants. Therefore, Figure 4a is utilized to fit the EIS data for the blank solution and for the addition of BHPE and KI separately, while Figure 4b is used to fit the EIS data for the simultaneous addition of BHPE and KI.



**Figure 4.** Fitting circuits: (a) blank, BHPE and KI, (b) BHPE+KI.

Table 2 displays the fitted data, wherein the symbols  $R_s$ ,  $R_f$ , and  $R_{ct}$  indicate the solution resistance, film resistance, and charge transfer resistance, respectively. The precision of the fitted data was evaluated using the chi-square test ( $\chi^2$ ), and all the  $\chi^2$  results had lower values, indicating a better fit [44]. The polarization resistance  $R_p$ , is calculated as the sum of  $R_f$  and  $R_{ct}$ . To account for non-ideal capacitive responses, the double-layer capacitor is replaced with the constant phase angle element (CPE). The impedance of the CPE ( $Z_{CPE}$ ) can be expressed as [45]:

$$Z_{CPE} = \frac{1}{Y_0(j\omega)^n} \quad (1)$$

where  $Y_0$  is used to describe the modulus of CPE,  $j$  and  $\omega$  represent the imaginary part and angular frequency, respectively, and  $n$  denotes the phase angle due to the inhomogeneity of the electrode surface. The radius of the impedance spectrum increases in the order of KI < BHPE < BHPE + KI. This means that the inhibitor creates a film with different levels of coverage on the electrode surface.

**Table 2.** EIS fitted data.

Inhibitor	C (mg/L)	$R_s$ ( $\Omega \text{ cm}^2$ )	$R_f$ ( $\Omega \text{ cm}^2$ )	$CPE_{dl}$		$R_{ct}$ ( $\Omega \text{ cm}^2$ )	$CPE_f$		$\eta_R$ (%)	$\chi^2$ $\times 10^{-2}$
				$Y_0 \times 10^{-6}$ ( $\text{S s}^n \text{ cm}^{-2}$ )	$n_1$		$Y_0 \times 10^{-6}$ ( $\text{S s}^n \text{ cm}^{-2}$ )	$n_2$		
Blank	0	6.1	–	147.6	0.971	18.6	–	–	–	6.377
	20	0.6	–	125	0.922	43.3	–	–	57.2	7.953
	50	0.6	–	89.2	0.922	63.2	–	–	70.6	5.624
BHPE	100	1.5	–	123.3	0.871	90.3	–	–	79.4	6.911
	200	0.1	–	122.4	0.856	114.6	–	–	83.8	6.220
	20	0.6	–	166.6	0.948	21.3	–	–	12.9	6.137
KI	50	5.7	–	145.5	0.956	25.0	–	–	25.6	7.955
	100	0.6	–	173.0	0.933	27.6	–	–	32.8	5.494
	200	0.6	–	188.1	0.936	22.7	–	–	18.2	5.039
BHPE + 100 mg/L KI	20	0.9	23.1	34.6	0.996	156.3	157.3	0.688	89.7	2.148
	50	0.9	18.6	35.3	0.998	201.2	155.5	0.681	91.6	2.071
	100	0.7	30.0	27.8	0.997	257.2	142.9	0.682	93.5	3.599
	200	0.7	25.2	23.9	0.996	306.8	163.1	0.657	94.4	3.175

The inhibition efficiency  $\eta_R\%$  can be determined by the polarization resistance  $R_p$ , which is calculated as shown in Equation (2) [46]. Where  $R_p^0$  and  $R_p$  correspond to the polarization resistances of the specimens in the blank and corrosion inhibitor-containing solutions, respectively.

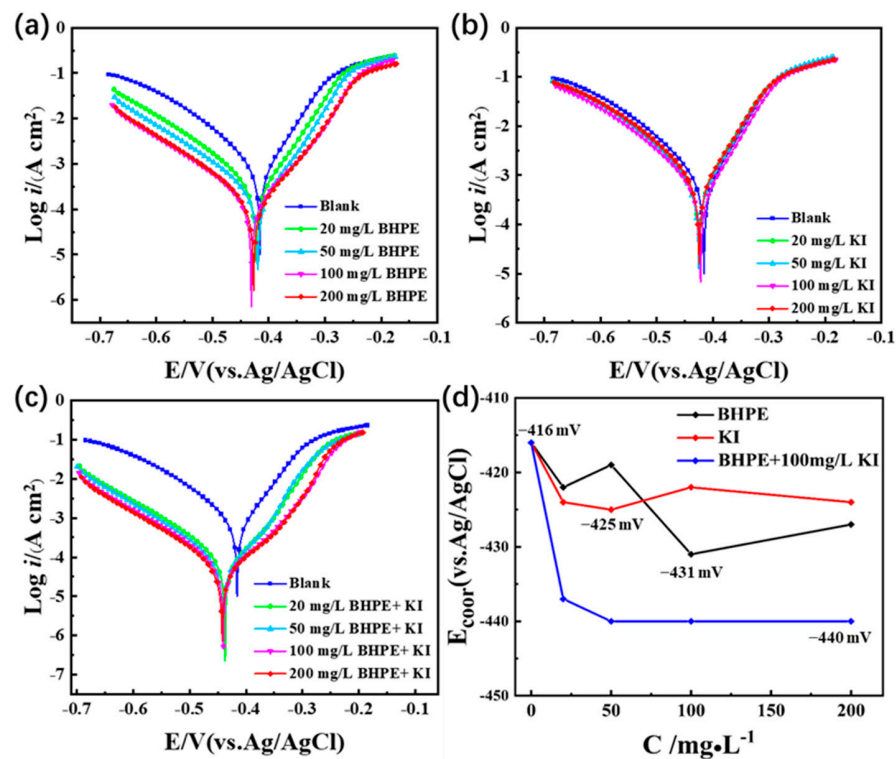
$$\eta_R(\%) = \frac{R_p - R_p^0}{R_p} \times 100 \quad (2)$$

Table 2 displays the increase in  $R_p$  and the decrease in  $CPE_{dl}$  with the addition of BHPE. The  $R_p$  increment can be attributed to the gradual integrity of the film formed on the electrode surface. The decrease in  $CPE_{dl}$  may be due to the decrease in the dielectric constant after the substitution of water molecules on the electrode surface [47].  $R_{ct}$  increases with increasing BHPE concentration, indicating that the charge transfer process controls the corrosion of mild steel. For BHPE alone,  $R_{ct}$  and  $\eta_R\%$  reach their maximum values, which are  $114.6 \Omega \text{ cm}^{-2}$  and 83.8%, respectively. When BHPE is combined with 100 mg/L KI, the maximum values of  $R_{ct}$  and  $\eta_R\%$  increase to  $306.8 \Omega \text{ cm}^{-2}$  and 94.4%, respectively. The results suggest that BHPE in 1 M HCl offers mild steel some protection against corrosion,

and its effectiveness increases when combined with KI, which can prevent corrosion more efficiently.

### 3.2.2. Polarization curve analysis

Figure 5a–c display the polarization curve plots for different concentrations of BHPE, KI and BHPE+KI, respectively. Figure 5a shows that the addition of BHPE shifted the curves of both the cathode and anode in both directions towards lower current density, but the slopes of the cathode and anode curves did not change significantly. This indicates that BHPE has an inhibitory effect on both the anodic and cathode processes corrosion electrochemistry, but does not change the mechanism of the reduction reaction of cathode hydrogen precipitation [48]. As indicated in Figure 5b, the shape of the polarization curves when KI alone is added is similar to that when BHPE alone is added, but the negative shifts in the curves at the cathode and anode are smaller. This indicates that KI has a relatively small corrosion inhibition performance.



**Figure 5.** Polarization curves for mild steel in 1 M HCl without and with different corrosion inhibitors: (a) BHPE, (b) KI, (c) BHPE + 100 mg/L KI, and (d) corrosion potential variation curves.

Figure 5c shows the polarization curves of BHPE combined with 100 mg/L KI as a corrosion inhibitor. The combination of BHPE and KI resulted in a noticeable shift in the polarization curves toward a decreased corrosion current density. This shift indicates a greater capacity for inhibiting mild steel corrosion when these two inhibitors are used in combination. Notably, the anodic curve slope in the polarization curve significantly alters within the polarization potential range of  $-400$  mV to  $-200$  mV. This change suggests that during this interval, a more comprehensive film forms on the surface of the mild steel, thus delaying the oxidation of iron at the anode [49].

The electrochemical parameters, such as the corrosion potential ( $E_{corr}$ ), corrosion current density ( $i_{corr}$ ), and cathodic and anodic slopes ( $\beta_c$ ,  $\beta_a$ ) of the polarization curves, are given in Table 3. The corrosion inhibition efficiency is calculated by the following equation [50]:

$$\eta_p(\%) = \frac{i_{corr}^0 - i_{corr}}{i_{corr}^0} \times 100 \quad (3)$$

**Table 3.** Electrochemical parameters of the polarization curves.

Inhibitor	<i>c</i> (mg/L)	<i>E</i> <sub>corr</sub> (mV vs. Ag/AgCl)	<i>i</i> <sub>corr</sub> (μA cm <sup>-2</sup> )	−β <sub>c</sub> (mV dec <sup>-1</sup> )	β <sub>a</sub> (mV dec <sup>-1</sup> )	η <sub>p</sub> (%)
Blank	0	−416	646.6	101.7	66.1	–
	20	−422	244.1	107.9	53.4	62.2
	50	−419	157.7	115.2	52.2	75.6
BHPE	100	−431	136.1	120.9	87.8	79.0
	200	−427	120.4	117.6	70.7	81.4
	20	−424	572.1	102.1	56.6	11.5
	50	−425	517.6	102.2	56.1	20.0
KI	100	−422	412.2	103.3	53.3	36.3
	200	−424	552.9	106.1	56.7	14.5
	20	−437	69.6	105.5	61.6	89.2
BHPE + 100 mg/LKI	50	−440	53.1	105.0	44.7	91.8
	100	−440	48.9	111.0	66.7	92.4
	200	−440	44.0	109.5	69.9	93.2

The variables  $i_{corr}^0$  and  $i_{corr}$  denote the corrosion current density prior to and subsequent to the introduction of a corrosion inhibitor into the solution, respectively.

Table 3 displays the impact of the BHPE concentration on the  $i_{corr}$  and  $\eta_p$ . It is evident that  $i_{corr}$  decreases and  $\eta_p$  increases with an increasing BHPE concentration, with the highest corrosion inhibition efficacy recorded at 81.4%. The use of only KI results in a decrease followed by an increase in  $i_{corr}$ , which hits its lowest point at a concentration of 100 mg/L, where the corresponding  $\eta_p$  value is 36.3%. When BHPE and 100 mg/L KI were used in combination, all the  $i_{corr}$  values decreased to below 69.6  $\mu\text{A cm}^{-2}$ , and the corrosion inhibitor efficiency remained at a high level, above 89.2%.

Figure 5d displays the change in corrosion potential after the addition of different corrosion inhibitors. The  $E_{corr}$  showed different degrees of negative shift after adding different corrosion inhibitors, and the degree of negative shift in  $E_{corr}$  was significantly higher when BHPE and KI were used simultaneously than when BHPE and KI were used alone. This once again indicates that BHPE and KI have a better synergistic effect. Further, the maximum negative shift value of  $E_{corr}$  was less than 85 mV, demonstrating that BHPE, KI and BHPE+KI are all hybrid corrosion inhibitors [51].

### 3.2.3. Synergy analysis

A synergy coefficient *S* was introduced to quantitatively evaluate the synergy between BHPE and KI. The value of *S* was calculated using the formula proposed by Aramaki and Hackerman [52]:

$$S = \frac{1 - \eta_A - \eta_B + \eta_A \eta_B}{1 - \eta_{AB}} \quad (4)$$

where  $\eta_A$ ,  $\eta_B$ , and  $\eta_{AB}$  represent the corrosion inhibition efficiency of BHPE, KI and BHPE+KI, respectively. When the parameter  $S = 1$ , there is no synergistic effect between BHPE and KI; when the parameter  $S > 1$ , synergy exists between BHPE and KI; and when the parameter  $S < 1$ , there is an antagonistic effect [53].

Figure 6 shows the synergistic coefficients obtained from the EIS and Tafel data for different concentrations of BHPE compounded with KI. It can be observed from Figure 6 that the synergistic coefficients exceeded 2 at BHPE concentrations of 20 mg/L and 50 mg/L, which indicates that BHPE has an extremely strong synergistic effect with KI at lower concentrations. As the concentration of BHPE increased, the coefficient of synergy gradually stabilized at approximately 1.7, which may be due to the saturation of BHPE adhesion at the mild steel interface. The fact that the synergistic coefficients (*S*) remain above 1 across all four concentration ranges highlights a significant synergistic interaction between BHPE and KI.

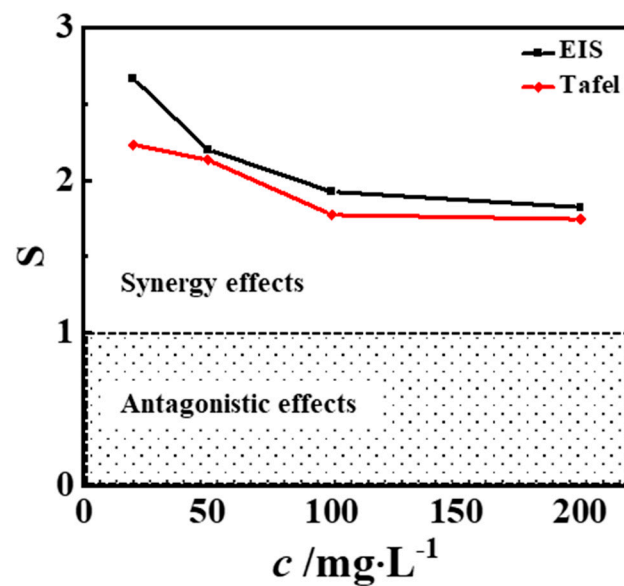


Figure 6. BHPE versus KI synergy coefficient in 1 M HCl for mild steel.

### 3.2.4. Adsorption Isotherm Study

Typically, the effectiveness of inhibitors in suppressing corrosion is closely related to their adsorption capacity, and adsorption isotherms can provide a means of assessing the adsorption capacity of corrosion inhibitors on metal surfaces. By utilizing the classical Langmuir adsorption isotherm, the data obtained from the EIS test on the BHPE and BHPE+KI in HCl solution was fitted, and the expression is as follows [54]:

$$\frac{C_{inh}}{\theta} = \frac{1}{K_{ads}} + C_{inh} \quad (5)$$

where  $C$  is the concentration of the corrosion inhibitor,  $\theta$  is the surface coverage, and  $K_{ads}$  is the adsorption equilibrium constant (its value is equivalent to the reciprocal of the Y-axis intercept of the adsorption isotherm). The results from the regression analysis are presented in Figure 7. The Langmuir adsorption isotherms exhibit high goodness of fit, as evidenced by the  $R^2$  coefficients of 0.99987 and 0.99998 for BHPE and BHPE+KI, respectively. The fact that both values are close to 1 and greater than 0.99 indicates that the Langmuir model is applicable. The  $K_{ads}$  values obtained for BHPE+KI were notably higher than those obtained for BHPE, suggesting that the addition of KI enhanced the adsorption of BHPE onto the mild steel surface, ultimately resulting in an improvement to its protective properties. One way to classify the type of adsorption by corrosion inhibitors is by using the standard Gibbs free energy of adsorption, which is calculated as follows [55]:

$$\Delta G_{ads}^0 = -RT \ln(10^3 K_{ads}) \quad (6)$$

where  $R$  represents the gas constant (8.314 J mol<sup>-1</sup> K<sup>-1</sup>),  $T$  is the absolute temperature (298.15 K), and  $10^3$  represents the concentration of water molecules (10<sup>3</sup> g/L). The value of  $\Delta G_{ads}^0$  can be obtained by substituting  $K_{ads}$  into Equation (6). A lower value of  $\Delta G_{ads}^0$  corresponds to a higher adsorption energy, indicating a higher corrosion inhibition efficiency. The values of  $\Delta G_{ads}^0$  for BHPE and BHPE+KI are  $-27.83$  and  $-32.99$ , respectively, indicating that BHPE+KI is more effective at inhibiting corrosion. Mixed adsorption is typically characterized by  $\Delta G_{ads}^0$  values between  $-40$  kJ/mol and  $-20$  kJ/mol. This indicates that the adsorption of BHPE and BHPE+KI on the surface of mild steel is composed of chemisorption and physisorption [56].

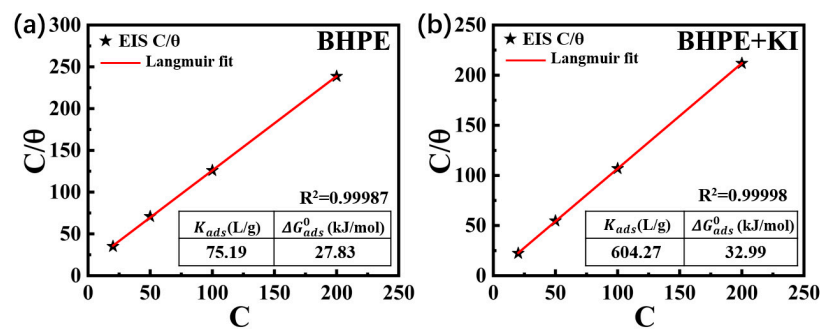


Figure 7. Langmuir adsorption isotherms for mild steel in the presence of: (a) BHPE and (b) BHPE+KI.

### 3.3. Surface Analysis

Figure 8a,c,e,g show the surface SEM images of mild steel after 2 h immersion in 1 M HCl solution without a corrosion inhibitor, with 500 mg/L BHPE, with 100 mg/L KI, and with 500 mg/L BHPE + 100 mg/L KI, respectively. It is evident that the surface of mild steel undergoes severe corrosion after immersion in the HCl solution without an inhibitor, with corrosion products distributed across the entire surface. Figure 8c,e show a significant reduction in corrosion on the mild steel surface compared to Figure 8a, but localized corrosion can still be observed. Figure 8g shows that the sandpaper polishing marks of mild steel are still clearly visible after immersion in a corrosion solution containing both 500 mg/L BHPE and 100 mg/L KI, and the corrosion level is greatly reduced. This indicates that BHPE and KI compounded in HCl solution have an excellent corrosion inhibition effect on mild steel.

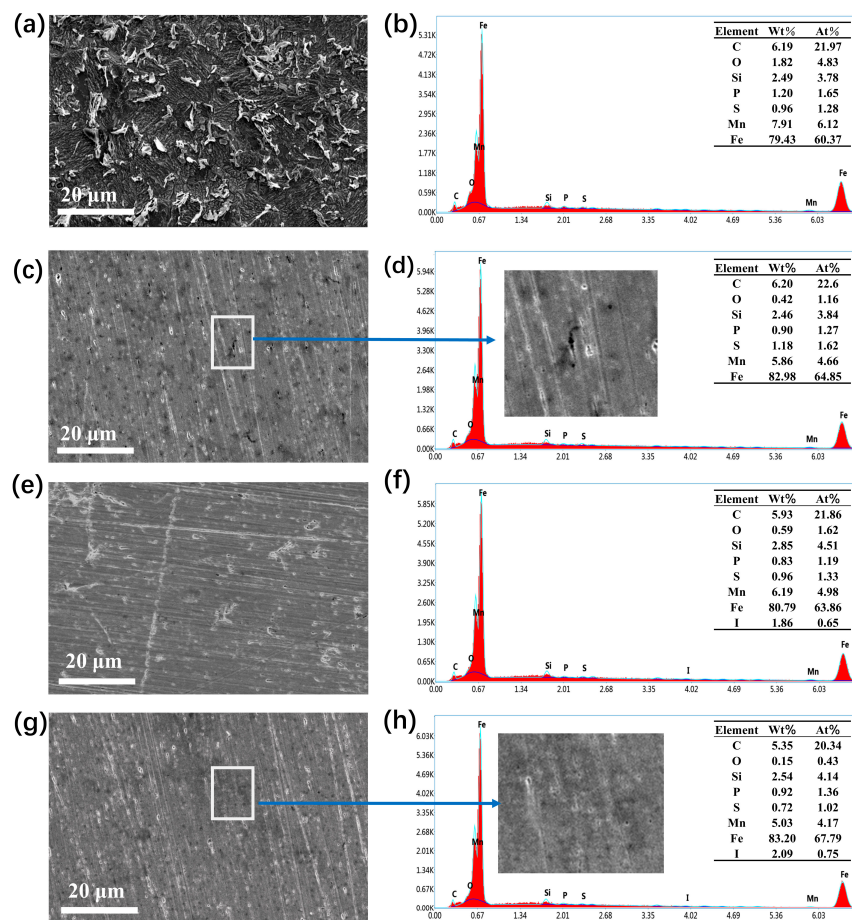


Figure 8. SEM images and EDX profiles of mild steel after 2 h immersion in 1 M HCl without and with different concentrations of corrosion inhibitors: (a,b) blank, (c,d) BHPE, (e,f) KI, (g,h) BHPE+KI.

The distribution of elements on the surface of mild steel after immersion in the corrosive solution was determined by EDX. Figure 8b,d,f,h show the corresponding EDX profiles. Upon comparison, it can be observed that the proportion of oxygen elements on the surface of mild steel is higher after immersion in the corrosion solution without a corrosion inhibitor. This is because in a corrosion solution without corrosion inhibitors, mild steel lacks protection and is oxidized more severely. In addition, low levels of iron were detected on the surface of mild steel exposed to HCl solutions without corrosion inhibitors. This is attributed to the fact that mild steel suffers more severe surface corrosion during immersion in HCl solutions without corrosion inhibitors. These phenomena indicate that the protective film formed on the surface of mild steel after the addition of corrosion inhibitors plays a good role in the protection of mild steel.

### 3.4. Theoretical Calculation Analysis

#### 3.4.1. QC Analysis

QC calculations can establish a correlation between the molecular structure of corrosion inhibitors and their corrosion inhibition effect, which helps to understand the adsorption mechanism of these inhibitors on metal surfaces [57]. To optimize the active components of BHPE, namely DM, DR, LP, DGA, TA, DG, DLX, and DF, the Dmol3 module was employed. Figure 9 presents the optimized molecular structures and frontier molecular orbital density distribution. The HOMO signifies the most electron-rich orbital in the molecule, whereas the LUMO represents the most electron-deficient orbital in the molecule.

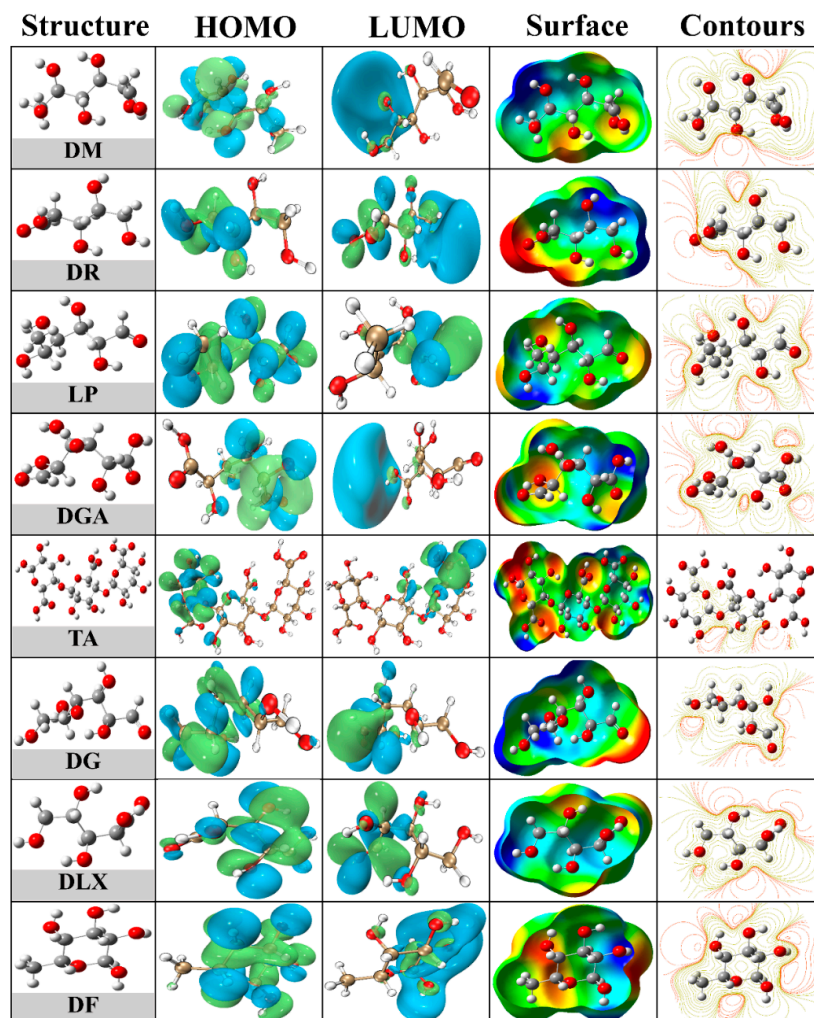


Figure 9. Optimized structure, FMO distribution, and OESP plot of eight monosaccharides.

Figure 9 illustrates the HOMO and LUMO diffusion patterns of the BHPE corrosion inhibitor molecule. Specifically, the HOMO diffusion pattern is concentrated near the C=O group and the O heteroatom, while the LUMO diffusion pattern is concentrated near the –COOH group of the  $\alpha$  carbon atom. This suggests that the molecule can potentially coordinate with metal ions via its carboxyl group. Moreover, the HOMO and LUMO distribution results indicate that the corrosion inhibitor interacts with ferrous orbitals primarily through oxygen atoms, which carry negative charges. Further insight into the molecule's spatial properties is provided by the isopotential diagram presented in Figure 9, which shows that the electron density is unevenly distributed across the molecule, indicating an asymmetrical structure. The OESP surface profile shows that the red areas are mainly located near the oxygen atoms, indicating that the corrosion inhibitor molecules may form coordination sites with iron atoms at these locations [58].

In addition, parameters such as the highest occupied orbital energy  $E_{HOMO}$  and the lowest unoccupied orbital energy  $E_{LUMO}$ , energy gap value  $\Delta E$ , electron affinity energy  $A$ , ionization potential  $I$ , overall hardness  $\gamma$ , electron transfer number  $\Delta N$ , electronegativity  $\chi$ , and dipole moment  $\mu$  of the active components of BHPE were also calculated by quantum chemistry and are listed in Table 4. The calculation equations are as follows [59,60]:

$$A = -E_{LUMO} \quad (7)$$

$$I = -E_{HOMO} \quad (8)$$

$$\chi = \frac{I + A}{2} \quad (9)$$

$$\gamma = \frac{I - A}{2} \quad (10)$$

$$\Delta N = \frac{\chi_{Fe} - \chi_{inh}}{2(\gamma_{Fe} + \gamma_{inh})} \quad (11)$$

$$\Delta E = I - A \quad (12)$$

**Table 4.** QC parameters of the eight monosaccharides.

Inhibitors	$E_{HOMO}$ (eV)	$E_{LUMO}$ (eV)	$\Delta E$ (eV)	I (eV)	A (eV)	$\chi$ (eV)	$\gamma$ (eV)	$\mu$ (Debye)	$\Delta N$
DM	−11.49	−0.79	10.70	11.49	0.79	6.14	5.35	4.55	0.08
DR	−6.87	−0.95	5.92	6.87	0.95	3.91	2.96	8.53	0.52
LP	−7.68	−1.64	6.04	7.68	1.64	4.66	3.02	1.40	0.39
DGA	−11.59	−0.87	10.71	11.59	0.87	6.23	5.36	4.06	0.07
TA	−7.01	−1.06	5.95	7.01	1.06	4.04	2.97	4.62	0.50
DG	−6.69	−1.39	5.30	6.69	1.39	4.04	2.65	8.53	0.56
DLX	−7.53	−1.54	5.99	7.53	1.54	4.54	3.00	3.22	0.41
DF	−7.46	−0.61	6.86	7.46	0.61	4.04	3.43	1.97	0.43

$\Delta E$  refers to the energy difference between *HOMO* and *LUMO* in the molecule. Specifically, the smaller the  $\Delta E$  value of the corrosion inhibitor, the easier it is for electrons to leap from *HOMO* to *LUMO* and, thus, undergo chemisorption. As shown in Table 4, the DG molecule among the active components of BHPE has the smallest  $\Delta E$  value, indicating that it may dominate in the inhibition of the metal corrosion process. Additionally, as seen in Table 4, both the  $\mu$  and  $\Delta N$  values of DG are the largest among all the active molecules. Many reports indicate that the values of  $\mu$  and  $\Delta N$  are also key indicators for judging the performance of corrosion inhibitors [61]. A larger  $\mu$  value of the molecule means a stronger intermolecular interaction, and a larger value of  $\Delta N$  means a more pronounced charge transfer in the reaction, both of which imply that the molecules are more likely to adsorb on the metal surface [62]. This further indicates that that DG is the most crucial factor in the mechanism of inhibiting metal corrosion.

### 3.4.2. MDS Analysis

Molecular dynamics simulation is an effective tool for investigating the mutual adsorption between corrosion inhibitor molecules and mild steel [63]. Figure 10 shows that the extract molecules finally adsorb on the metal surface in a parallel adsorption manner, and the parallel adsorption approach results in a higher coverage by the protective film formed on the metal surface, thus reducing corrosion attack. Moreover, the parallel adsorption technique allows more active sites on the steel surface to be in contact with the corrosion inhibitor molecules. This phenomenon contributes to better formation of coordination bonds, resulting in higher corrosion inhibition efficiency. The interaction energy ( $E_{interact}$ ) between each component single molecule and the steel substrate is calculated as follows [64]:

$$E_{intercat} = E_{tot} - E_{sub} - E_{inh} \quad (13)$$

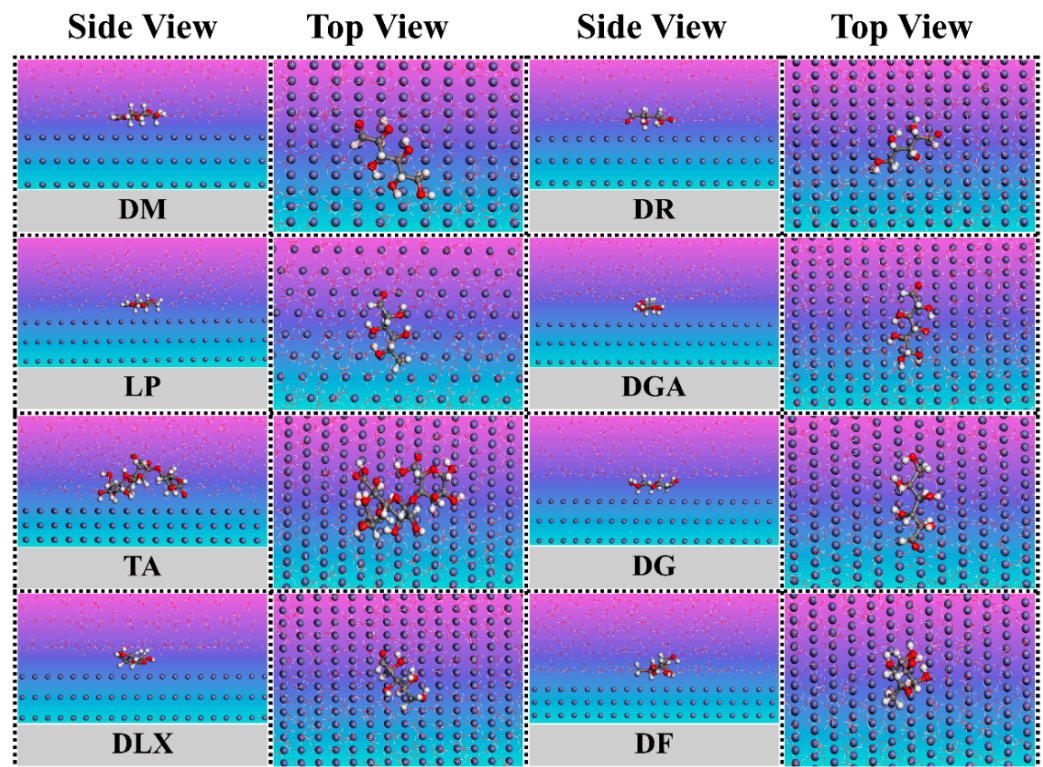


**Figure 10.** Stable adsorption configurations of eight monosaccharides on the surface of Fe (110).

$E_{tot}$  represents the total energy of the whole system,  $E_{inh}$  is the total energy of the corrosion inhibitor, and  $E_{sub}$  represents the energy of all the  $H_2O$  molecules and the mild steel substrate. In addition, the binding energy ( $E_{binding}$ ) is obtained from the negative value of the interaction energy.

$$E_{binding} = -E_{interact} \quad (14)$$

Table 5 demonstrates the energy parameters of the binding energy for each component. Among them, the binding energy of DG is 1438.5 kJ/mol, which is much larger than that of other monosaccharide molecules. Therefore, it can be judged that the adsorption of DG is more likely to occur on the surface of mild steel. The analytical results are consistent with the quantum chemical calculations.

**Table 5.** Energy parameters of eight monosaccharides on the surface of Fe (110).

	DM (kJ/mol)	DR (kJ/mol)	LP (kJ/mol)	DGA (kJ/mol)	TA (kJ/mol)	DG (kJ/mol)	DLX (kJ/mol)	DF (kJ/mol)
$E_{top}$	−5615.2	−5664.4	−5834.6	−4949.7	−2554.9	−4805.6	−710.0	−4960.9
$E_{sub}$	−5438.1	−5523.0	−5621.9	−4715.7	−2896.7	−3976.3	−921.5	−4685.8
$E_{inh}$	307.5	245.1	229.7	256.6	661.4	609.3	510.3	184.0
$E_{interact}$	−484.6	−386.6	−442.4	−490.5	−319.5	−1438.5	−298.9	−459.2
$E_{binding}$	484.6	386.6	442.4	490.5	319.5	1438.5	298.9	459.2

### 3.5. Corrosion Inhibition Mechanism

The corrosion mechanism of mild steel in HCl and the corrosion inhibition mechanism of BHPE and KI are shown in the schematic diagram in Figure 11. As depicted in Figure 11a, mild steel immersed in HCl solution will undergo an electrochemical reaction in which the iron at the anode will be oxidized to  $Fe^{2+}$  and the cathode will undergo hydrogen precipitation to produce  $H_2$ . Meanwhile,  $Cl^-$  in HCl solution will be attracted to the positively charged ( $Fe^{2+}$ ) metal surface through electrostatic interactions.

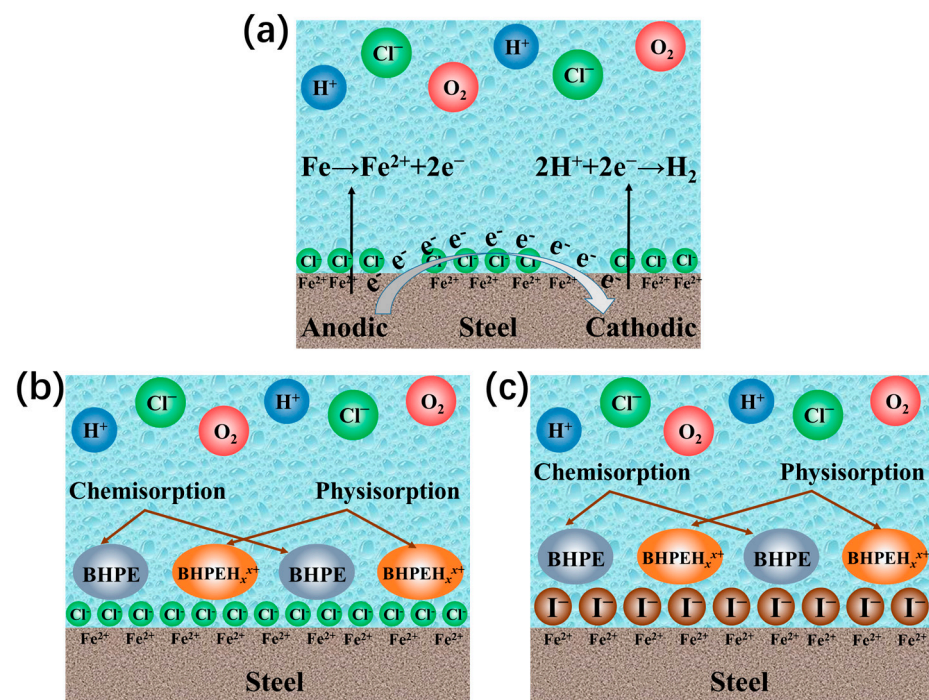


**Figure 11.** Diagram of the corrosion mechanism and corrosion inhibitor mechanism of mild steel in HCl with and without a corrosion inhibitor: (a) without corrosion inhibitor, (b) BHPE, (c) BHPE+KI.

As shown in Figure 11b, the corrosion on the mild steel surface was inhibited by the addition of BHPE. This is because the lone pair electrons of O atoms in BHPE in HCl solution can form coordination bonds with the empty orbitals of Fe atoms, resulting in chemisorption. Second, the O atoms in BHPE will combine with  $H^+$  in HCl solution to form protonated  $BHPEH_x^{X+}$ , which will not only reduce the concentration of  $H^+$  but also electrostatically adsorb  $Cl^-$  on the steel surface because of its positive charge, which is a physical adsorption process. The simultaneous existence of physical adsorption and chemical adsorption makes BHPE form a relatively complete adsorption film, thus providing protection to the mild steel.

As shown in Figure 11c, the synergistic mechanism of KI and BHPE is demonstrated. The large size and easy polarization of iodide ions ( $I^-$ ) after the addition of KI makes its adsorption ability on the steel surface stronger than that of  $Cl^-$ , thus replacing  $Cl^-$  to form a more stable and wider range of  $I^-$  adsorption layers on the steel surface. The  $I^-$

adsorption layer gives the steel surface a more uniform negative charge and, thus, it is to adsorb more protonated BHPEH<sub>x</sub><sup>x+</sup>. This leads to the formation of larger and more uniform corrosion inhibitor coverage on the mild steel surface.

#### 4. Conclusions

BHPE was prepared by hot water extraction and freeze drying using *Benincasa hispida* rind as the raw material. The synergistic mechanism of BHPE with KI for corrosion inhibition of mild steel in 1 M HCl was investigated using experiments and theoretical calculations. The main findings from this work are as follows:

- (1) HPLC confirmed that the main components of BHPE are sugar complexes, which contain more O and polar groups –OH, which are favorable for the formation of coordination bonds with Fe. FTIR confirmed that BHPE has the basic characteristics of an efficient corrosion inhibitor.
- (2) The EIS data showed that both BHPE and KI have a certain corrosion inhibition effect on mild steel in 1 M HCl solution. The maximum corrosion inhibition efficiency was 83.8% and 32.8% when BHPE and KI concentrations were 200 mg/L and 100 mg/L, respectively. When 200 mg/L BHPE and 100 mg/L KI were used simultaneously, the maximum corrosion inhibition efficiency reached 94.4%. The Tafel curve confirmed that the BHPE and KI complexes were mixed corrosion inhibitors.
- (3) The synergy coefficients (S) of BHPE and KI were greater than 1 for all concentration conditions, confirming the existence of good synergy between BHPE and KI. The adsorption isotherm study confirmed that both BHPE and BHPE+KI follow the Langmuir adsorption model and confirmed that the adsorption process for BHPE on a mild steel surface consists of physical and chemical adsorption.
- (4) QC confirms the presence of active adsorption sites in the main components of BHPE. The MDS simulation results show that BHPE is adsorbed on the mild steel surface in a parallel manner, resulting in a more complete and stable protective film formed on the metal surface. The results of the theoretical calculations effectively support the experimental data conclusions.

**Author Contributions:** Conceptualization, Q.W. and D.S.; methodology, Q.W.; software, C.Z.; validation, Q.Z. and X.Z.; formal analysis, C.Z. and Y.S.; investigation, Q.W. and C.Z.; resources, Z.Y. and X.L.; data curation, C.Z. and Y.S.; writing—original draft preparation, Q.W.; writing—review and editing, D.S.; visualization, C.Z.; supervision, Q.W.; project administration, D.S.; funding acquisition, D.S. All authors have read and agreed to the published version of the manuscript.

**Funding:** This work was supported by the Science and Technology Innovation Program of “the construction of the Chengdu-Chongqing economic circle” (No. KJJCX2020050), the Research Foundation of Chongqing University of Science and Technology (No. ckrc2020025), the Natural Science Foundation of China (Nos. 51778097, 52178458), the Innovation Program for Graduate Students of Chongqing University of Science and Technology (No. YKJCX2220604, No. YKJCX2220605), and the Science and Technology Research Program of Chongqing Municipal Education Commission (Grant No. KJQN202201518).

**Institutional Review Board Statement:** Not applicable.

**Informed Consent Statement:** Not applicable.

**Data Availability Statement:** Not applicable.

**Conflicts of Interest:** The authors declare no conflict of interest.

#### References

1. Wang, Q.; Zheng, H.; Liu, L.; Zhang, Q.; Wu, X.; Yan, Z.; Sun, Y.; Li, X. Insight into the anti-corrosion behavior of *Reineckia Carne* leaves extract as an eco-friendly and high-efficiency corrosion inhibitor. *Ind. Crops Prod.* **2022**, *188*, 115640. [CrossRef]
2. Medupin, R.O.; Ukoba, K.O.; Yoro, K.O.; Jen, T.-C. Sustainable approach for corrosion control in mild steel using plant-based inhibitors: A review. *Mater. Today Sustain.* **2023**, *22*, 100373. [CrossRef]

3. Zhang, Q.H.; Xu, N.; Jiang, Z.N.; Liu, H.F.; Zhang, G.A. Chitosan derivatives as promising green corrosion inhibitors for carbon steel in acidic environment: Inhibition performance and interfacial adsorption mechanism. *J. Colloid Interface Sci.* **2023**, *640*, 1052–1067. [[CrossRef](#)] [[PubMed](#)]
4. Li, E.; Li, Y.; Liu, S.; Yao, P. Choline amino acid ionic liquids as green corrosion inhibitors of mild steel in acidic medium. *Colloids Surf. A* **2023**, *657*, 130541. [[CrossRef](#)]
5. Bedair, M.A.; Elaryian, H.M.; Gad, E.S.; Alshareef, M.; Bedair, A.H.; Aboushabha, R.M.; Fouda, A.E.S. Insights into the adsorption and corrosion inhibition properties of newly synthesized diazinyll derivatives for mild steel in hydrochloric acid: Synthesis, electrochemical, SRB biological resistivity and quantum chemical calculations. *RSC Adv.* **2022**, *13*, 478–498. [[CrossRef](#)]
6. Motawea, M.M. Experimental, computational studies and spectroscopic analysis on the effective Aeluropus lagopoides extract as water-soluble green corrosion inhibitor for carbon steel in 1 M HCl solution. *J. Adhes. Sci. Technol.* **2021**, *36*, 1633–1665. [[CrossRef](#)]
7. Kaya, F.; Solmaz, R.; Geçibesler, İ.H. Investigation of adsorption, corrosion inhibition, synergistic inhibition effect and stability studies of Rheum ribes leaf extract on mild steel in 1 M HCl solution. *J. Taiwan Inst. Chem. Eng.* **2023**, *143*, 104712. [[CrossRef](#)]
8. Shafek, S.H.; Ghiaty, E.A.; El Basonry, N.M.; Badr, E.A.; Shaban, S.M. Preparation of zwitterionic ionic surfactants-based sulphonyl for steel protections: Experimental and theoretical insights. *Zeitschrift für Physikalische Chemie* **2023**, *237*, 1–33. [[CrossRef](#)]
9. Kellal, R.; Left, D.B.; Azzi, M.; Zertoubi, M. Insight on the corrosion inhibition performance of Glebionis coronaria plant extract in various acidic mediums. *J. Appl. Electrochem.* **2022**, *53*, 811–832. [[CrossRef](#)]
10. Gabsi, M.; Ferkous, H.; Delimi, A.; Boublia, A.; Boulechfar, C.; Kahlouche, A.; Darwish, A.S.; Lemaoui, T.; Benguerba, Y. The curious case of polyphenols as green corrosion inhibitors: A review on their extraction, design, and applications. *Environ. Sci. Pollut. Res. Int.* **2023**, *30*, 59081–59105. [[CrossRef](#)]
11. Zhang, R.; Chen, H.; Yu, Q.; Zhang, Y.; Liu, F.; Wang, F.; Chen, X.; Liu, Y. Extraction of bioactive compounds from cinnamon residues with deep eutectic solvents and its molecular mechanism. *Hem. Eng. Sci.* **2023**, *273*, 118630. [[CrossRef](#)]
12. Wang, Q.; Wang, R.; Zhang, Q.; Zhao, C.; Zhou, X.; Zheng, H.; Zhang, R.; Sun, Y.; Yan, Z. Application of Biomass Corrosion Inhibitors in Metal Corrosion Control: A Review. *Molecules* **2023**, *28*, 2832. [[CrossRef](#)] [[PubMed](#)]
13. Benzbiria, N.; Thoume, A.; Echihi, S.; Belghiti, M.E.; Elmakssoudi, A.; Zarrouk, A.; Azzi, M.; Zertoubi, M. Coupling of experimental and theoretical studies to apprehend the action of benzodiazepine derivative as a corrosion inhibitor of carbon steel in 1M HCl. *J. Mol. Struct.* **2023**, *1281*, 135139. [[CrossRef](#)]
14. Bhardwaj, N.; Sharma, P.; Kumar, V. Phytochemicals as steel corrosion inhibitor: An insight into mechanism. *Corros. Rev.* **2021**, *39*, 27–41. [[CrossRef](#)]
15. Wan, S.; Wei, H.; Quan, R.; Luo, Z.; Wang, H.; Liao, B.; Guo, X. Soybean extract firstly used as a green corrosion inhibitor with high efficacy and yield for carbon steel in acidic medium. *Ind. Crops Prod.* **2022**, *187*, 115354. [[CrossRef](#)]
16. Berrissoul, A.; Ouarhach, A.; Benhiba, F.; Romane, A.; Guenbour, A.; Dikici, B.; Bentiss, F.; Zarrouk, A.; Dafali, A. Assessment of corrosion inhibition performance of origanum compactum extract for mild steel in 1 M HCl: Weight loss, electrochemical, SEM/EDX, XPS, DFT and molecular dynamic simulation. *Ind. Crops Prod.* **2022**, *187*, 115310. [[CrossRef](#)]
17. Nazari, A.; Ramezanzadeh, B.; Guo, L.; Dehghani, A. Application of green active bio-molecules from the aquatic extract of Mint leaves for steel corrosion control in hydrochloric acid (1M) solution: Surface, electrochemical, and theoretical explorations. *Colloids Surf. A* **2023**, *656*, 130540. [[CrossRef](#)]
18. Deyab, M.A. Egyptian licorice extract as a green corrosion inhibitor for copper in hydrochloric acid solution. *J. Ind. Eng. Chem.* **2015**, *22*, 384–389. [[CrossRef](#)]
19. Haldhar, R.; Kim, S.-C.; Prasad, D.; Bedair, M.A.; Bahadur, I.; Kaya, S.; Dagdag, O.; Guo, L. Papaver somniferum as an efficient corrosion inhibitor for iron alloy in acidic condition: DFT, MC simulation, LCMS and electrochemical studies. *J. Mol. Struct.* **2021**, *1242*, 130822. [[CrossRef](#)]
20. Liu, L.; Wu, X.; Wang, Q.; Yan, Z.; Wen, X.; Tang, J.; Li, X. An overview of microbiologically influenced corrosion: Mechanisms and its control by microbes. *Corros. Rev.* **2022**, *40*, 103–117. [[CrossRef](#)]
21. Khadiri, M.; Idouhli, R.; Bennouna, M.A.; Aityoub, A.; Abouelfida, A.; Benyaïch, A. Contribution to understanding synergistic effect of Punica granatum extract and potassium iodide as corrosion inhibitor of S355 steel. *Corros. Rev.* **2021**, *39*, 137–148. [[CrossRef](#)]
22. Solomon, M.M.; Essien, K.E.; Loto, R.T.; Ademosun, O.T. Synergistic corrosion inhibition of low carbon steel in HCl and H<sub>2</sub>SO<sub>4</sub> media by 5-methyl-3-phenylisoxazole-4-carboxylic acid and iodide ions. *J. Adhes. Sci. Technol.* **2021**, *36*, 1200–1226. [[CrossRef](#)]
23. Thomas, A.; At, J.R.; Joseph, A. Extended protection of mild steel in molar HCl using the Garcinia Indica fruit rind extract (GIW) and iodide ions; electrochemical, thermodynamic and kinetic studies. *J. Indian Chem. Soc.* **2021**, *98*, 100167. [[CrossRef](#)]
24. Wang, H.; Deng, S.; Du, G.; Li, X. Synergistic mixture of Eupatorium adenophora spreng leaves extract and KI as a novel green inhibitor for steel corrosion in 5.0 M H<sub>3</sub>PO<sub>4</sub>. *J. Mater. Res. Technol.* **2023**, *23*, 5082–5104. [[CrossRef](#)]
25. Wan, S.; Zhang, T.; Chen, H.; Liao, B.; Guo, X. Kapok leaves extract and synergistic iodide as novel effective corrosion inhibitors for Q235 carbon steel in H<sub>2</sub>SO<sub>4</sub> medium. *Ind. Crops Prod.* **2022**, *178*, 114649. [[CrossRef](#)]
26. Li, X.; Deng, S.; Fu, H.; Xie, X. Synergistic inhibition effects of bamboo leaf extract/major components and iodide ion on the corrosion of steel in H<sub>3</sub>PO<sub>4</sub> solution. *Corros. Sci.* **2014**, *78*, 29–42. [[CrossRef](#)]
27. Nkiko, M.O. Evaluating the Deterioration of Galvanized Steel in an Acidic Medium using Pinus Oocarpa Seed Extract as Inhibitor. *Port. Electrochim. Acta* **2022**, *40*, 79–87. [[CrossRef](#)]

28. Li, X.; Deng, S. Synergistic inhibition effect of walnut green husk extract and potassium iodide on the corrosion of cold rolled steel in trichloroacetic acid solution. *J. Mater. Res. Technol.* **2020**, *9*, 15604–15620. [[CrossRef](#)]
29. Rodriguez-Torres, A.; Valladares-Cisneros, M.G.; Saldana Heredia, A.; Gonzalez-Rodriguez, J.G. KI effects on corrosion inhibition for 1018 steel in acid media using *Medicago sativa*. *Front. Chem.* **2022**, *10*, 1032522. [[CrossRef](#)]
30. Tang, M.; Li, X.; Deng, S.; Lei, R. Synergistic inhibition effect of *Mikania micrantha* extract with KI on steel corrosion in H<sub>2</sub>SO<sub>4</sub> solution. *J. Mol. Liq.* **2021**, *344*, 117926. [[CrossRef](#)]
31. Wang, K.; Sheng, X.; Chen, X.; Zhu, X.; Yang, C. Characterization and antioxidant activities of polysaccharide extracted from *Benincasa hispida* var. How. *Food Sci. Technol.* **2022**, *42*, e88421. [[CrossRef](#)]
32. Islam, M.T.; Quispe, C.; El-Kersh, D.M.; Shill, M.C.; Bhardwaj, K.; Bhardwaj, P.; Sharifi-Rad, J.; Martorell, M.; Hossain, R.; Al-Harrasi, A.; et al. A Literature-Based Update on *Benincasa hispida* (Thunb.) Cogn.: Traditional Uses, Nutraceutical, and Phytopharmacological Profiles. *Oxid. Med. Cell. Longev.* **2021**, *2021*, 6349041. [[CrossRef](#)] [[PubMed](#)]
33. Wang, Q.; Yang, X.; Zhu, C.; Liu, G.; Han, W.; Sun, Y.; Qian, L. Valorization of Polysaccharides from *Benincasa hispida*: Physicochemical, Moisturizing, and Antioxidant Skincare Properties. *Front. Pharmacol.* **2022**, *13*, 912382. [[CrossRef](#)] [[PubMed](#)]
34. Palamthodi, S.; Kadam, D.; Lele, S.S. Physicochemical and functional properties of ash gourd/bottle gourd beverages blended with jamun. *J. Food Sci. Technol.* **2019**, *56*, 473–482. [[CrossRef](#)]
35. Chaouiki, A.; Chafiq, M.; Ko, Y.G.; Al-Moubaraki, A.H.; Thari, F.Z.; Salghi, R.; Karrouchi, K.; Bougrin, K.; Ali, I.H.; Lgaz, H. Adsorption Mechanism of Eco-Friendly Corrosion Inhibitors for Exceptional Corrosion Protection of Carbon Steel: Electrochemical and First-Principles DFT Evaluations. *Metals* **2022**, *12*, 101598. [[CrossRef](#)]
36. Ke, H.; Taylor, C.D. Density Functional Theory: An Essential Partner in the Integrated Computational Materials Engineering Approach to Corrosion. *Corrosion* **2019**, *75*, 708–726. [[CrossRef](#)]
37. Dagdag, O.; Safi, Z.; Wazzan, N.; Erramli, H.; Guo, L.; Mkadmh, A.M.; Verma, C.; Ebenso, E.E.; El Gana, L.; El Harfi, A. Highly functionalized epoxy macromolecule as an anti-corrosive material for carbon steel: Computational (DFT, MDS), surface (SEM-EDS) and electrochemical (OCP, PDP, EIS) studies. *J. Mol. Liq.* **2020**, *302*, 112535. [[CrossRef](#)]
38. Wang, Q.; Zhang, Q.; Liu, L.; Zheng, H.; Wu, X.; Li, Z.; Gao, P.; Sun, Y.; Yan, Z.; Li, X. Experimental, DFT and MD evaluation of *Nandina domestica* Thunb. extract as green inhibitor for carbon steel corrosion in acidic medium. *J. Mol. Struct.* **2022**, *1265*, 133367. [[CrossRef](#)]
39. Aquino-Torres, E.; Camacho-Mendoza, R.L.; Gutierrez, E.; Rodriguez, J.A.; Feria, L.; Thangarasu, P.; Cruz-Borbolla, J. The influence of iodide in corrosion inhibition by organic compounds on carbon steel: Theoretical and experimental studies. *Appl. Surf. Sci.* **2020**, *514*, 145928. [[CrossRef](#)]
40. Wang, Q.; Wu, X.; Zheng, H.; Xiao, X.; Liu, L.; Zhang, Q.; Gao, P.; Yan, Z.; Sun, Y.; Li, Z.; et al. Insight into anti-corrosion behavior of *Centipeda minima* leaves extract as high-efficiency and eco-friendly inhibitor. *Colloids Surf. A* **2022**, *640*, 128458. [[CrossRef](#)]
41. Liao, B.; Ma, S.; Zhang, S.; Li, X.; Quan, R.; Wan, S.; Guo, X. Fructus cannabis protein extract powder as a green and high effective corrosion inhibitor for Q235 carbon steel in 1 M HCl solution. *Int. J. Biol. Macromol.* **2023**, *239*, 124358. [[CrossRef](#)] [[PubMed](#)]
42. Sannaiah, P.N.; Alva, V.D.P.; Bangera, S. An integrated electrochemical and theoretical approach on the potency of *Senegalia rugata* leaf extract as a novel inhibitor for mild steel in acidic medium. *J. Appl. Electrochem.* **2021**, *52*, 395–412. [[CrossRef](#)]
43. Wang, Q.; Liu, L.; Zhang, Q.; Wu, X.; Zheng, H.; Gao, P.; Zeng, G.; Yan, Z.; Sun, Y.; Li, Z.; et al. Insight into the anti-corrosion performance of *Artemisia argyi* leaves extract as eco-friendly corrosion inhibitor for carbon steel in HCl medium. *Sustain. Chem. Pharm.* **2022**, *27*, 100710. [[CrossRef](#)]
44. Liao, B.; Luo, Z.; Wan, S.; Chen, L. Insight into the anti-corrosion performance of *Acanthopanax senticosus* leaf extract as eco-friendly corrosion inhibitor for carbon steel in acidic medium. *J. Ind. Eng. Chem.* **2023**, *117*, 238–246. [[CrossRef](#)]
45. El-Asri, A.; Rguiti, M.M.; Jmiai, A.; Oukhrib, R.; Bourzi, H.; Lin, Y.; Issami, S.E. *Carissa macrocarpa* extract (ECM) as a new efficient and ecologically friendly corrosion inhibitor for copper in nitric acid: Experimental and theoretical approach. *J. Taiwan Inst. Chem. Eng.* **2023**, *142*, 104633. [[CrossRef](#)]
46. Salinas-Solano, G.; Porcayo-Calderon, J.; Martinez de la Escalera, L.M.; Canto, J.; Casales-Diaz, M.; Sotelo-Mazon, O.; Henao, J.; Martinez-Gomez, L. Development and evaluation of a green corrosion inhibitor based on rice bran oil obtained from agro-industrial waste. *Ind. Crops Prod.* **2018**, *119*, 111–124. [[CrossRef](#)]
47. Zarei, A.; Dehghani, A.; Guo, L.; Ramezanzadeh, B. Pepper extract effectiveness as a natural inhibitor against corrosion of steel samples (SS) in 1 M hydrochloric acid; Theoretical (DFT calculation–MD simulation), thermodynamic, and electrochemical-surface studies. *Ind. Crops Prod.* **2022**, *189*, 115839. [[CrossRef](#)]
48. Huang, L.; Zhao, Q.; Li, H.-J.; Wang, J.-Y.; Wang, X.-Y.; Wu, Y.-C. Investigation of adsorption and corrosion inhibition property of Hyperoside as a novel corrosion inhibitor for Q235 steel in HCl medium. *J. Mol. Liq.* **2022**, *364*, 120009. [[CrossRef](#)]
49. Mansha, M.; Madhan Kumar, A.; Adesina, A.Y.; Obot, I.B.; Khan, M. A novel trans-esterified water soluble hyperbranched polymer for surface protection of X60 steel: Experimental and theoretical approach. *J. Mol. Liq.* **2022**, *349*, 118091. [[CrossRef](#)]
50. Sowmyashree, A.S.; Somya, A.; Kumar, S.; Rao, S.; Jayaprakash, G.K. Discotic anthraquinones as novel corrosion inhibitor for mild steel surface. *J. Mol. Liq.* **2022**, *347*, 118194. [[CrossRef](#)]
51. Ganjoo, R.; Sharma, S.; Thakur, A.; Assad, H.; Kumar Sharma, P.; Dagdag, O.; Berisha, A.; Seydou, M.; Ebenso, E.E.; Kumar, A. Experimental and theoretical study of Sodium Cocoyl Glycinate as corrosion inhibitor for mild steel in hydrochloric acid medium. *J. Mol. Liq.* **2022**, *364*, 119988. [[CrossRef](#)]

52. Gk, S.; Jacob, J.M.; P, R.; Raj, A., Jr. Synergistic effect of salts on the corrosion inhibitive action of plant extract: A review. *J. Adhes. Sci. Technol.* **2020**, *35*, 133–163. [[CrossRef](#)]
53. Chang, H.-D.; Wu, B.-E.; Chandra Sil, M.; Yang, Z.-H.; Chen, C.-M. Study of synergy of monoethanolamine and urea on copper corrosion inhibition in alkaline solution. *J. Mol. Liq.* **2022**, *359*, 119344. [[CrossRef](#)]
54. Hassan, R.M.; Ibrahim, S.M. Performance and efficiency of methyl-cellulose polysaccharide as a green promising inhibitor for inhibition of corrosion of magnesium in acidic solutions. *J. Mol. Struct.* **2021**, *1246*, 131180. [[CrossRef](#)]
55. Verma, D.K.; Kazi, M.; Alqahtani, M.S.; Syed, R.; Berdimurodov, E.; Kaya, S.; Salim, R.; Asatkar, A.; Haldhar, R. N-hydroxybenzothioamide derivatives as green and efficient corrosion inhibitors for mild steel: Experimental, DFT and MC simulation approach. *J. Mol. Struct.* **2021**, *1241*, 130648. [[CrossRef](#)]
56. Yang, X.; Fu, S.; Wang, Q.; Sun, Q.; Zhang, J.; Peng, Y.; Liang, Z.; Li, J. Protective behaviour of naphthylamine derivatives for steel reinforcement in the simulated concrete pore solutions: Detailed experimental and computational explorations. *J. Mol. Struct.* **2022**, *1270*, 133898. [[CrossRef](#)]
57. Obot, I.B.; Macdonald, D.D.; Gasem, Z.M. Density functional theory (DFT) as a powerful tool for designing new organic corrosion inhibitors. Part 1: An overview. *Corros. Sci.* **2015**, *99*, 1–30. [[CrossRef](#)]
58. Zhang, Q.H.; Hou, B.S.; Li, Y.Y.; Lei, Y.; Wang, X.; Liu, H.F.; Zhang, G.A. Two amino acid derivatives as high efficient green inhibitors for the corrosion of carbon steel in CO<sub>2</sub>-saturated formation water. *Corros. Sci.* **2021**, *189*, 109596. [[CrossRef](#)]
59. Haque, J.; Srivastava, V.; Quraishi, M.A.; Singh Chauhan, D.; Lgaz, H.; Chung, I.-M. Polar group substituted imidazolium zwitterions as eco-friendly corrosion inhibitors for mild steel in acid solution. *Corros. Sci.* **2020**, *172*, 108665. [[CrossRef](#)]
60. Zhang, W.; Nie, B.; Wang, M.; Shi, S.; Gong, L.; Gong, W.; Pang, H.; Liu, X.; Li, B.; Feng, Y.; et al. Chemically modified resveratrol as green corrosion inhibitor for Q235 steel: Electrochemical, SEM, UV and DFT studies. *J. Mol. Liq.* **2021**, *343*, 117672. [[CrossRef](#)]
61. Farhadian, A.; Rahimi, A.; Safaei, N.; Shaabani, A.; Abdouss, M.; Alavi, A. A theoretical and experimental study of castor oil-based inhibitor for corrosion inhibition of mild steel in acidic medium at elevated temperatures. *Corros. Sci.* **2020**, *175*, 108871. [[CrossRef](#)]
62. Saady, A.; Rais, Z.; Benhiba, F.; Salim, R.; Ismaily Alaoui, K.; Arrousse, N.; Elhajjaji, F.; Taleb, M.; Jarmoni, K.; Kandri Rodi, Y.; et al. Chemical, electrochemical, quantum, and surface analysis evaluation on the inhibition performance of novel imidazo[4,5-b] pyridine derivatives against mild steel corrosion. *Corros. Sci.* **2021**, *189*, 109621. [[CrossRef](#)]
63. Majd, M.T.; Ramezanzadeh, M.; Bahlakeh, G.; Ramezanzadeh, B. Steel corrosion lowering in front of the saline solution by a nitrogen-rich source of green inhibitors: Detailed surface, electrochemical and computational studies. *Constr. Build. Mater.* **2020**, *254*, 119266. [[CrossRef](#)]
64. Singh, A.; Ansari, K.R.; Ituen, E.; Guo, L.; Abdul Wahab, M.; Quraishi, M.A.; Kong, X.; Lin, Y. A new series of synthesized compounds as corrosion mitigator for storage tanks: Detailed electrochemical and theoretical investigations. *Constr. Build. Mater.* **2020**, *259*, 120421. [[CrossRef](#)]

**Disclaimer/Publisher's Note:** The statements, opinions and data contained in all publications are solely those of the individual author(s) and contributor(s) and not of MDPI and/or the editor(s). MDPI and/or the editor(s) disclaim responsibility for any injury to people or property resulting from any ideas, methods, instructions or products referred to in the content.